CrossMark

Cobalt-doped zincblende–wurtzite mixed-phase ZnO photocatalyst nanoparticles with high activity in visible spectrum

Biju Mani Rajbongshi, S.K. Samdarshi*

Solar and Energy Materials Laboratory, Department of Energy, Tezpur University, Tezpur 784028, Assam, India

ABSTRACT

The photoactivity of metal-oxide nanoparticles can be elevated and extended in the visible range through doping, sensitization, nanostructuration, and phase mixing. The present work reports synthesis of highly photoactive cobalt-doped mixed phase/biphasic zinc oxide nanoparticles with zinc-blende and wurtzite phases. The photoactivity of the nanoparticles, assessed through photocatalytic degradation kinetics of methylene blue and phenol, shows over 3 and 1.5 times more visible light photoactivity than monophasic (wurtzite) undoped ZnO and doped Co-ZnO counterparts, respectively. The increase in the activity is mainly attributed to red-shift in the absorption spectrum due to doping. But in the mixed phase (biphasic) Co-ZnO it is further complemented by the synergy of the interacting phases at the homojunction and the increase in oxygen vacancies at the surface which ensure availability of more photogenerated carriers by contributing in their generation and/or separation.

The synthesis of the novel mixed-phase photocatalyst has been done through a sol–gel based facile and single-step process wherein cobalt plays the unique role of dopant-cum-substrate.

© 2013 Elsevier B.V. All rights reserved.

1. Introduction

Activity of a photocatalyst nanoparticle can be elevated and extended in the visible range using a number of strategies such as doping, sensitization, nanostructuration and phase mixing. While crystalline monophasic nanoparticles have been widely studied under doped/sensitized condition with robust and predictable characteristics, their biphasic/polyphasic counterparts, now being developed offer unique opportunities due to their novel characteristics which are useful for photocatalysis applications. Such a study on ZnO has not been reported because of obvious reasons. Out of the three known structural polymorphs of ZnO – wurtzite (hexagonal, WZ), zincblende (cubic, ZB), and rocksalt (cubic, RS) the wurtzite phase has received maximum attention of researchers due to the highest thermodynamic stability and ease of synthesis compared to pristine ZB and RS phases which are metastable. Thus getting a mixed phase ZnO with one or more metastable phase(s) becomes incrementally more challenging. Each of these metastable monophases, due to its unpredictable physical and chemical properties, has been projected to be more exciting than the stable counterparts [1]. Due to its lower ionicity and higher crystallographic symmetry than the other polymorphs, ZB-ZnO is expected to have the advantage of low carrier scattering, higher

doping efficiency and higher optical gain [2] which, consequently, may impart superior optical and electronic properties to it. Due to these ZB-ZnO nanostructures are being considered as the future for development of a number of low-cost efficient devices such as LEDs, lasers, sensors [3], electronic memories [4], electrochromic displays [5] and applications such as photocatalysis [6], photovoltaics, spintronics [7], and piezoelectricity [8]. Lu et al. [6] concentrated on the study of dependence of photoactivity on hierarchical morphology of nanostructures. To the best of the authors' knowledge the photocatalytic performance study on mixed phase (biphasic) ZnO with ZB-ZnO has not been reported so far.

In general the attempts to synthesize metastable monophase of ZnO has puzzled the researchers because of the existence of mixed phase homojunctions in the yield. The attempts to synthesize ZB-ZnO employing techniques such as molecular beam epitaxy [9,10], metalorganic chemical vapour deposition [11], thermal oxidation of ZnS [12,13], sol–gel [14], thermal evaporation [15], solvothermal method [6], refluxing [16], and pulse laser deposition method [17] have invariably yielded biphasic nanomaterials such as ZB phase with WZ subdomains or vice versa [2,9,11–13,16,18,19]. Nevertheless, two important outcomes of these efforts are – One, these efforts have resulted in growth of novel ZB nanostructures like nano-tetrapods [20,21], nano-helices [22], nano-wires [5,15], and hierarchical pyramid made of nano-sheets [6] all with subdomains of the phase other than the bulk; and, two, they have further evidenced the existence of mixed phase. Caroff et al. [4] in their work on InAs polymorphs predicted interesting effects and

* Corresponding author. Tel.: +91 9435490522.
E-mail address: drsksamdarshi@rediffmail.com (S.K. Samdarshi).

futuristic applications in mixed phase nanostructures in general. Recently Nair et al. have demonstrated the existence of synergistic effect of the homojunction of two coexisting phases in a photoactive titania nano-material [23–25]. In the case of ZnO the growth of metastable ZB phase always yields such junctions. This provides an opportunity to study the photoactivity of such a material. It may be noted here that in majority of the synthesis methods the approach has been to use an appropriate substrate (sapphire, silica) to grow ZB-ZnO directly or through thermal oxidation of epitaxial ZnS grown on the substrate [2].

The band gap of ZnO phases ranges between 3.27 eV (WZ) and 3.19 eV (ZB) [26,27] making it suitable for UV light activity only [28]. To extend its activity to visible range, doping by a range of transition metals like Fe, Ni, Co, and Mn, has been attempted. Out of these Co is preferred because ionic radius of cobalt (0.58 Å) matches with zinc (0.60 Å) and, also, because it results in significant red-shift [29] in the absorption spectrum of ZnO. Notably all the previous studies explicitly report on WZ-ZnO only.

In the present work an attempt is made to synthesize Co-doped ZnO using sol–gel method. Surprisingly the method yields a biphasic ZnO without the use of a substrate or precursor. As stated earlier, the ZB phase invariably grows only on matching cubic zincblende substrates irrespective of the techniques used. It appears that this method has provided a novel route wherein cobalt works both as dopant and substrate. It calls for an attempt to investigate the conditions under which Co can double as a substrate as well. The existence of two phases in the sample further prompted us to investigate the existence of synergy, if any, in biphasic Co-doped-ZnO, which has never been reported so far, to be used for an application such as photocatalysis. It has been done through demonstration of visible/UV light photocatalytic degradation of standard probe materials in the presence of the synthesized biphasic Co-ZnO (WZ–ZB) and its comparison with monophasic doped and undoped ZnO (WZ) samples. The comparison of the kinetics indeed indicates toward the existence of a correlation between the photoactivity and the synergy of the two phases in addition to the increased presence of oxygen vacancies and doping enabled red-shift in the biphasic Co-ZnO (WZ–ZB) material. Further this work also attempts to explain the synergy in terms of the interface model.

2. Experimental

2.1. Material synthesis

The chemical used for synthesis of Co doped ZnO were zinc acetate dihydrate $(CH3COO)_2 Zn \cdot 2H_2O$, cobalt nitrate hexahydrate $(CoNO_3)_2 \cdot 6H_2O$, sodium hydroxide pellets NaOH and ethanol. All these materials were purchased from Merck (India). Double distilled water was used in all the processes.

Initially the solution of zinc, prepared by dissolving 1.1 g of zinc acetate in 20 mL of ethanol [30] and 1 wt% of cobalt nitrate solution in 10 mL of ethanol were mixed under constant stirring at room temperature. The pH of the solution was maintained in the alkaline range by adding 0.05 mol of NaOH. After continuous stirring for 8 h the material was dried at 80 °C and then calcined at 400 °C and 500 °C at 4 °C/min ramping rate to get the two Co-doped samples. Pure ZnO sample was also synthesized by the same process, without adding cobalt nitrate solution, at a calcination temperature of 400 °C.

2.2. Characterization

X-ray diffraction (XRD) pattern was recorded on diffractometer (Rigaku Miniflex, Japan) using Cu Kα radiation at 30 kV and 450 W
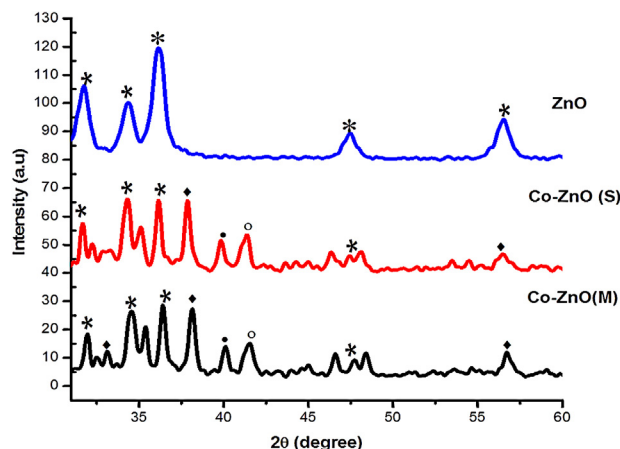

Fig. 1. XRD patterns of ZnO, Co-ZnO in single and mixed phase with peaks identified for WZ-ZnO (*), ZB-ZnO (♦), cubic CoO (●) and Co (○).

at a scan rate of 0.05 2θ/s. Scanning electron microscope (SEM) images were taken using scanning electron microscope (6390LV, Jeol, Japan) operated at an accelerating voltage of 15 kV. Energy dispersive X-ray analysis (EDAX) was done using the EDAX attachment (Oxford Instruments, UK) to the same system. The transmission electron microscope (TEM), model JEM-100CX II (JEOL Japan), was used to study the internal structure and morphology. The spectral response of the catalyst material was evaluated using UV–vis diffuse reflectance spectra using a UV–DRS spectrophotometer (Shimadzu UV-2200, Japan) with diffuse reflectance attachment. The photoluminescence spectrum was recorded using a photoluminescence spectrometer (LS55, Perkin Elmer, USA) for studying the trap states and FT-IR studies were done using a FT-IR spectrometer (Nicolet Impact I-410, USA). The XPS analysis was done by ESCA Instrument, VSW, UK. The thermo-gravimetric analysis (TGA) was done by the thermo-gravimetric analyzer (model STA-6000, Perkin Elmer, USA).
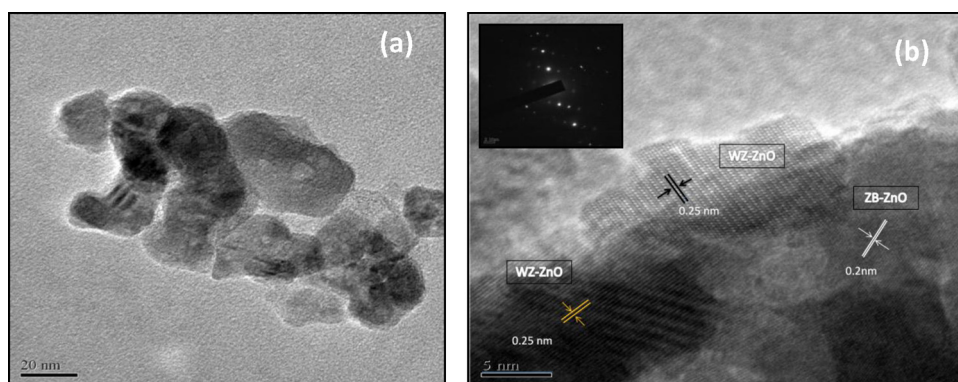
2.3. Photocatalytic activity test

The photocatalytic activity of the synthesized nano-material was studied using two aqueous probe pollutants – methylene blue (MB) and phenol. Phenol was used to exclude the effect of synergy of sensitization in the visible light photoactivity of the material in the presence of MB dye. The degradation kinetics was studied under visible light irradiation using a source (Radium, Relogen PAR30, China) with visible spectrum (see Supporting Information Fig. S6). The visible irradiance at the reactor surface was 121 W/m² (measured by Research radiometer, International light, USA with detectors SD 005 and SD 033). Catalyst loading was 0.5 g/L and the average reaction temperature was maintained at 38 °C. The adsorption–desorption equilibrium was ensured by keeping the catalyst loaded MB and phenol solution in dark for 1 h. Sampling was done at an interval of 15 min after irradiating the sample with visible light. The change in the concentration of the sample was recorded by correlating it with the absorbance of the sample, measured using UV–vis spectrophotometer (Shimadzu 1700, Japan), at wavelength 270 and 650 nm, respectively, for phenol and MB.

3. Results and discussion

3.1. Structure and morphology

Fig. 1 shows the XRD of the Co-ZnO calcined at temperature 400 °C and 500 °C. It can be observed that Co-ZnO, calcined at 500 °C, shows peaks corresponding to pure wurtzite phase of ZnO

Fig. 2. TEM (a) and HR-TEM (b) image of Co-ZnO(M) and the corresponding SEAD pattern (inset, (b)).

(JCPDF = 891397) with some peaks from CoO (JCPDF = 750419). Interestingly the sample calcined at 400 °C shows an extra peak at $2\theta = 33.045°$, which matches with the peaks of zincblende ZnO (JCPDF = 652880) and also with zincblende phase of Co-ZnO (JCPDF = 81-2295-99) systems, respectively. The process adopted in this work did not yield cobalt doped monophasic ZB-ZnO phase, instead it resulted in the growth of a biphasic material. The undoped sample also calcined at 400 °C, yielded monophasic system having wurtzite phase only. This indicates toward the important role of the dopant cobalt in the formation of ZB phase. Henceforth, the Co-ZnO samples calcined at 400 °C and 500 °C are referred to as Co-ZnO(M) and Co-ZnO(S), respectively. The pure wurtzite ZnO sample calcined at 400 °C is referred to as WZ-ZnO or ZnO. Particle sizes for Co-ZnO(M), Co-ZnO(S) and pristine ZnO were estimated using the Scherrer formula ($d = k\lambda/\beta\cos\theta$, where d is the crystallite size, λ is the X-ray wavelength (CuK$_\alpha$ = 0.15406 nm), k is the shape factor (0.9), β is the full width at half maximum of the most intense peak and θ is the diffraction angle) and are given in Table 1. For biphasic Co-ZnO(M) it is found to be 16.4 nm for the wurtzite subdomain (using the [0 0 2] plane) and 29 nm for the zincblende subdomain (using the [1 1 1] plane). The structural parameters for wurtzite sub-domain are estimated to be $a = 3.17$ Å and $c = 5.49$ Å, respectively, which are different from those of reported WZ-ZnO parameters (JCPDF = 891397, $a = 3.25$ Å, $c = 5.213$ Å) indicating substitution of Co^{2+} of smaller ionic radius for Zn^{2+}. But the value of structural parameter for zincblende subdomain was estimated to be $a = 4.67$ Å which accords well with the value reported for ZB-ZnO (JCPDF = 652880, $a = 4.629$ Å). For Co-ZnO(S) the particle size was 13.3 nm which corroborates the earlier reports that WZ has smaller particles size than ZB phase of ZnO. The undoped WZ-ZnO sample yielded the particle size of 11.3 Å.

3.1.1. Formation of cobalt-doped polytypic ZnO homojunction with metastable phase

As mentioned earlier that all the attempts to synthesize metastable ZB phase through a number of techniques essentially employed a substrate/precursor of suitable matching phase. Although the pure ZB phase eluded all the earlier reports including the present one, it is notable that the present work did not use either a precursor or a substrate. Instead it appears that the dopant played an important role here. It is important to note here that CoO

Table 1
Particle size of the samples.

SL no.	Sample	Particle size (nm)
1	ZnO	11.3 (WZ)
2	Co-ZnO(S)	13.3(WZ)
3	Co-ZnO(M)	16.4 (WZ), 29 (ZB)

has a cubic ZB lattice. But the formation of ZB-cobalt must precede so that it is available as substrate for the in situ growth of ZB-ZnO on it. To explain this basic process of formation of this material there is a need to understand the conditions for synthesis of ZB phase of the dopant cobalt first. The synthesis of ZB phase of CoO, first demonstrated by Redman and Stewart [31] and concluded more recently [32], indicates that it forms at a temperature of 290 °C with the subsequent advent of its transformation to WZ phase at 310 °C. Importantly the transformation of ZB-ZnO to WZ-ZnO commences at 377 °C [15]. It may be noted that the transformation temperature of CoO is below the transformation temperature of ZB-ZnO to WZ-ZnO phase making the ZB-CoO available as a substrate. Thus it is possible that the CoO, after its formation during calcination, plays the role of in situ precursor under the coincidental existence of the suitable control parameters. Thus the present work may provide a novel single step route to synthesize a number of metastable structures as it ensures the interaction of species at an intermediate stage before their transition to global minimum with least free energy conforming to the Ostwald's step rule. Moreover presence of cobalt may help in reducing the band gap to get the much-needed red-shift. To the best of the knowledge of the authors such a process to synthesize ZnO with ZB phase has not been reported before. However it probably resembles the topological synthesis method reported earlier by Pueyo et al. [1] or a method employed to study the shape evolution in ZnO by Yang et al. [33]. As an extension of the presented work the synthesis of such materials with other dopant-cum-precursors is being carried out by the authors.

The TEM micrograph, shown in Fig. 2a reveals its particle size to be identical to the XRD estimate of about 20–30 nm. Fig. 2b reveals the lattice planes of two clearly identifiable phases with the d-spacing 0.25 nm and 0.20 nm corresponding to WZ and ZB phase, respectively, indicating the existence of biphasic homojunction. SAED pattern (inset) of Co-ZnO(M) shows the particles to be of crystalline nature. The SEM micrograph of Co-ZnO(S) and Co-ZnO(M) (S1#) show indistinguishable agglomerated structures for both. EDAX spectrum (S2A) for Co-ZnO(M) and mappings (S2B#) for both the samples confirm the presence and uniform distribution of the elements zinc, cobalt and oxygen in them.

3.2. Optical properties

Comparing the UV-DRS spectrum (Fig. 3) it is seen that both the Co-doped samples show red shift with respect to the pure WZ-ZnO. The band gap for Co-ZnO(S), and Co-ZnO(M) are estimated using Tauc's relation to be 2.69 eV and 2.5 eV, respectively, whereas that of the undoped WZ-ZnO it is 3.25 eV. The values for Co-ZnO(S) and WZ-ZnO are in accordance with the earlier reports [24]. The band gap of Co-ZnO(M) is more red-shifted, which may only be due to the presence of the ZB phase as the cobalt concentration in both
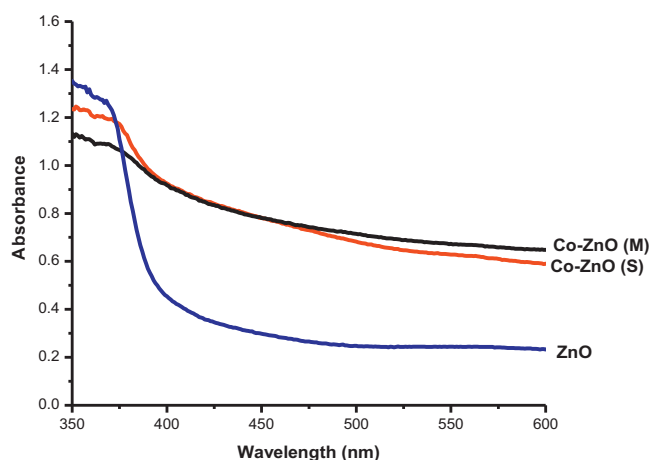
Fig. 3. UV-DRS of pure ZnO, Co-ZnO(S) and Co-ZnO(M).

the samples was identical. However ZB phase is expected to have higher solubility for cobalt and may also be responsible for more red-shift, but is not conclusively depicted in the UV spectrum.

The photoluminescence spectra of pristine WZ-ZnO, wurtzite Co-ZnO(S) and mixed Co-ZnO(M), shown in Fig. 4, have band-edge emission in the UV/blue region near 380 nm corresponding to ZnO. The weak emissions in the visible region from 420 nm to 541 nm originate mainly from the oxygen vacancy and the intrinsic and extrinsic surface defects in pristine ZnO and Co-ZnO. Here the quenching in the Co-ZnO emission peaks with respect to pristine ZnO may be attributed to reduction in oxygen vacancy due to cobalt doping. Additionally it may also be ascribed to enhanced separation of photo-induced charge-carriers (explained later to substantiate their photocatalytic performance) at the interface of WZ–ZB interface in the Co-ZnO(M). The red-shift is mainly due to the band-edge shift ascribed to substitution of Zn^{2+} ions by Co^{2+} ions.

3.3. Analysis of functional groups

FT-IR study to investigate the functional groups in the samples (Fig. 5) shows a band around $450\,cm^{-1}$ corresponding to ZnO and another at around $857\,cm^{-1}$ to CoO. The bands at $2900\,cm^{-1}$ and 1380 and $1640\,cm^{-1}$ are assignable to C—H vibration and C=O stretching modes, respectively [34]. Thermal stability of the material and the crystalline structure was established by TGA analysis (S3#). It was found that all the samples showed a weight loss at $150\,°C$ corresponding to water loss followed by a loss at $250\,°C$, which may be assigned to loss of organic groups mainly in the samples calcined at a relatively low temperature of $400\,°C$. Although
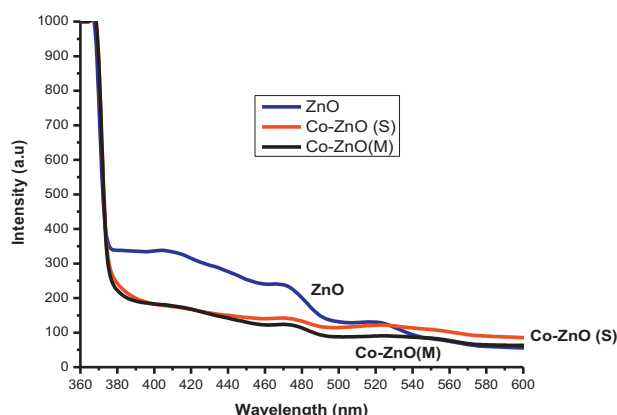

Fig. 4. PL spectrum of pure ZnO, Co-ZnO(S) and Co-ZnO(M).

this loss is not visible in Co-ZnO(S) and undoped WZ-ZnO, a small loss visible at $400\,°C$ in Co-ZnO(M) is attributable to loss of impurity ions and a possible phase transition of the ZB to a denser WZ phase.

3.4. Surface electronic structure

Fig. 6a shows the full-range XPS spectra of the pristine ZnO, Co-ZnO(S) and Co-ZnO(M) revealing the only Zn and O peaks. Co peaks are not visible in the spectra which may be due to the low doping concentration of Co. But the high resolution 2p state spectra of Co, both for Co-ZnO(S) and Co-ZnO(M), reveal two clear peaks ascribable to cobalt in metallic (Co^o) and oxidized (Co^{n+}) state, respectively (Fig. 6b). The metallic Co peaks at 778 eV and 793 eV are assigned to $^2P_{3/2}$ and $^2P_{1/2}$, respectively. The higher binding energy peaks located at 780 eV and 796 eV may be attributed, respectively, to $^2P_{3/2}$ and $^2P_{1/2}$ peaks of oxidized Co. This shift is visible when there is a charge transfer between Co-species [35]. The additional satellite peaks at 786 eV and 803 eV are visible only when Co^{2+} is present [36,37]. In Co-ZnO(S) the oxidized Co peaks are dominant in the spectrum indicating toward only a minor contribution of metallic Co. It has been found that Co^o and Co^{2+} may be present in the surface region depending on synthesis conditions. From the high resolution XPS spectrum of Zn 2p state (Fig. 6c) it can be seen that $^2P_{3/2}$ peak appears at 1022.5 eV for ZnO and Co-ZnO(S). But there is a shift of the $^2P_{3/2}$ peak to higher energy in Co-ZnO(M) which is ascribed to the doping or incorporation of Co into the ZnO matrix and the resultant formation of cubic zincblende ZnO and which results in charge transfer from Zn^{2+} to Co species [38]. Fig. 6d shows the O 1s peaks which can be deconvoluted into three components centered at about 529–530 eV, 531–532 eV and 532–533 eV for O^{2-} ions corresponding ZnO lattice with adequate oxygen, ZnO lattice with oxygen-deficiency and the surface bonded O—H or O_2, respectively [39]. The ratio of the first two peaks corresponding to the ZnO lattice with deficient and adequate oxygen provides the information about the concentration of oxygen vacancy in ZnO. Accordingly the ratio 1.11 (ZnO), 1.266 (Co-ZnO(S)) and 1.528 (Co-ZnO(M)) indicate that the oxygen vacancy is more in doped samples and the mixed phase sample has a very high concentration of oxygen vacancy. But the result is contrary to the result obtained through PL. In that case it appears from the XPS spectra that the oxygen vacancy is present in the surface region only.

3.5. Photocatalytic activity

Visible light photocatalytic performance of the samples was evaluated in terms of the kinetics of degradation of both methylene blue (MB) dye and phenol. The rate constants were calculated by plotting ln C/Co vs. time (Fig. 8). The blank MB showed detectable self-degradation compared to phenol. The WZ-ZnO sample showed little photoactivity to degrade both MB and phenol, which increased substantially for Co-doped samples (Fig. 7) and is in accordance with earlier reports [40,41]. The most interesting result was that of the Co-ZnO(M) sample which showed higher activity than Co-ZnO(S). In the case of Co-ZnO(S) the high activity may be attributed to increased visible light absorption and presence of surface oxygen vacancy as the sample has reasonably low level of bulk oxygen vacancy. In fact the increase in the oxygen vacancy at the surface in the doped samples, as seen in XPS, is responsible for high photoactivity. This holds true for Co-ZnO(M) also for which XPS peaks show further increase in surface oxygen vacancy. Thus the increase in photoactivity may be attributed to the presence of homojunction and resultant oxygen vacancy in biphasic Co-ZnO(M), which play an important role through reduction of recombination of photogenerated carriers mainly by efficient separation and transport of the carriers in the present case. The increase in the rate constant of
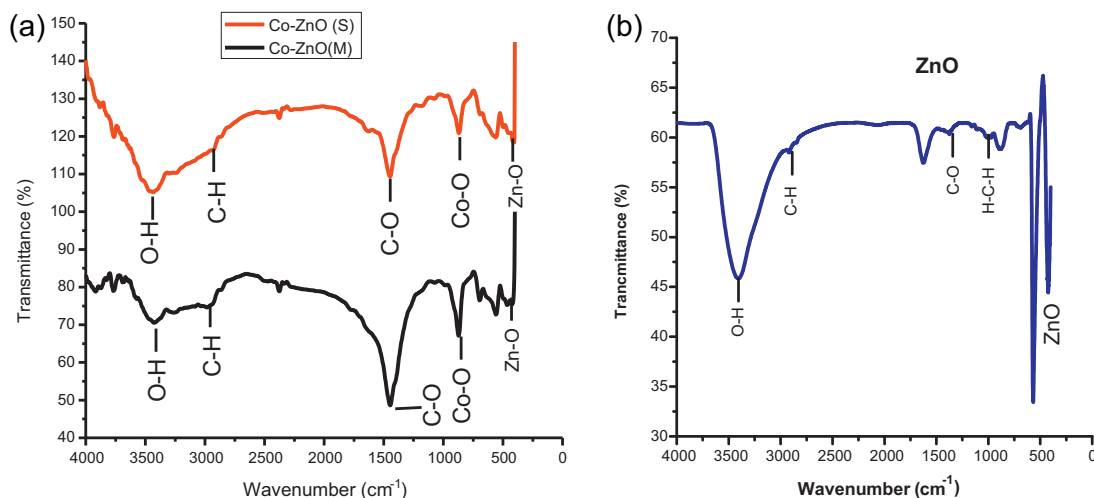
Fig. 5. FT-IR spectrum of (a) Co-ZnO(S), Co-ZnO(M) and (b) pure ZnO.

Co-ZnO(M) is 3–4 times with respect to WZ-ZnO and more than 1.5 times with respect to Co-ZnO(S) (Table 2) which correlates well with the increase in oxygen vacancies. The role of the two phases in separation of photogenerated carriers in the sample may be explained by considering the model proposed earlier in context of homojunction of biphasic titania. The two phases in intimate contact in the sample Co-ZnO(M) have their equilibrium junction band-edges as dictated by their respective work function, carrier type, carrier density and band gap. Accordingly since the electron affinity of WZ-ZnO is −4.3 eV [42] and as per the density functional
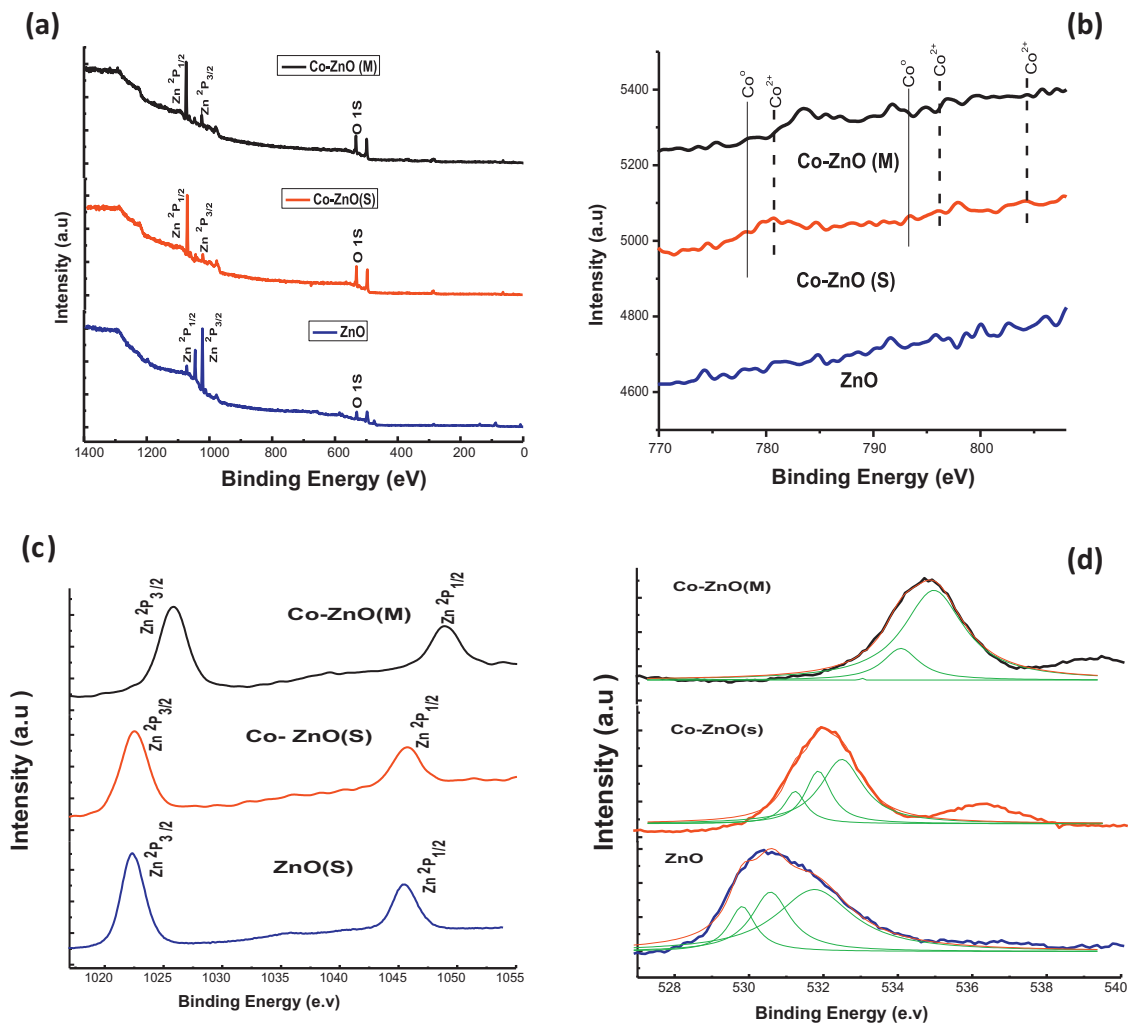

Fig. 6. XPS spectrum of full scan (a), high resolution spectra of Co 2p state (b), Zn 2p state (c) and O 1s state (d).
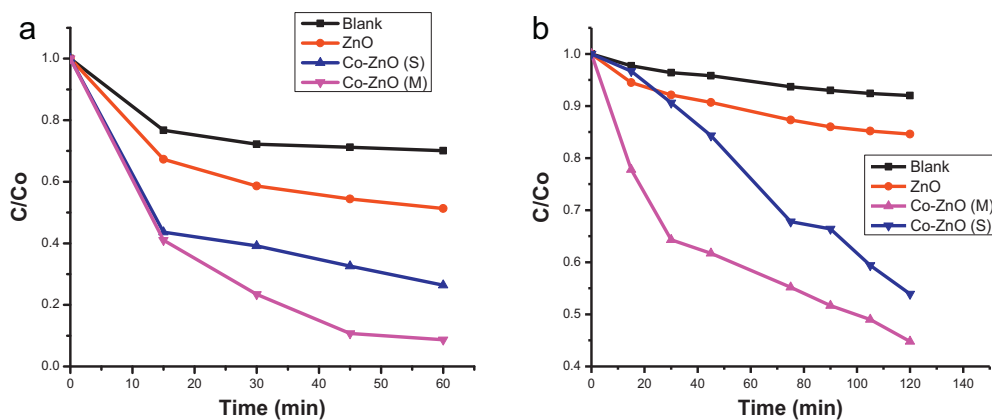
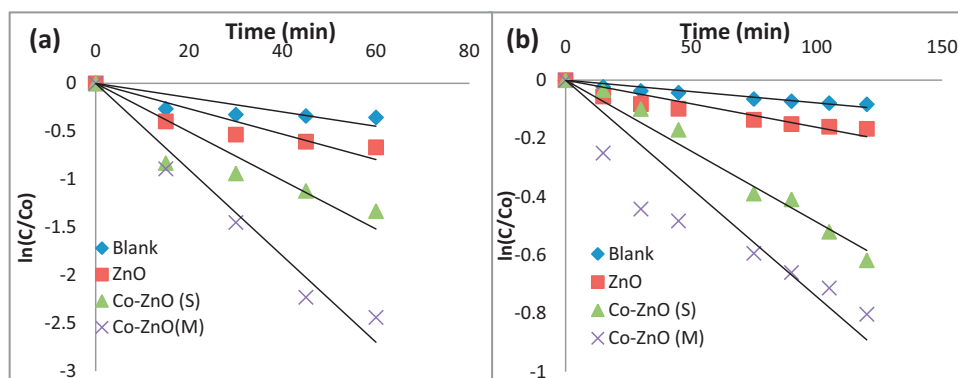**Fig. 7.** Degradation curve of (a) MB and (b) phenol under visible light.

Fig. 8. ln C/Co vs. time plot for determination of rate constants of degradation of (a) MB and (b) phenol under visible light.

Table 2
Photocatalytic degradation rate constant and photonic efficiency of the samples.

Catalyst sample	Rate constant (min^{-1})		Standard deviation of rate constant in phenol degradation	Photonic efficiency (%)	
	MB	Phenol		MB	Phenol
ZnO	0.013	0.0016	–	0.014	0.002
Co-ZnO(S)	0.025	0.0049	±0.0011	0.021	0.007
Co-ZnO(M)	0.045	0.0074	±0.0016	0.027	0.008

theory estimates the conduction and valence band edge of ZB-ZnO are shifted by −0.147 eV and −0.037 eV, respectively [43], the equilibrium interfacial band structure would be as shown in Fig. S4. The intrinsic barrier potential between the phases not only expedites and restricts the movement of the two species of the charge carriers in opposite directions it also reduces their recombination probability.

4. Conclusions

Thus the present work successfully demonstrates a facile single-step route for synthesis of a biphasic cobalt doped ZnO having WZ and metastable ZB phases showing high visible light photocatalytic activity compared to monophasic Co-ZnO as well as undoped wurtzite ZnO, both having wurtzite phase only. The activity of such biphasic systems is explained in terms of reduced recombination mainly due to surface oxygen vacancy and favorable charge separation and transport characteristics of the interface.

The facile single-step route for synthesis of a novel WZ–ZB biphasic homojunction of cobalt doped ZnO has been proposed. The process of synthesis has been explained in terms of temperature of formation/transformation of the phases of the dopant cobalt and the bulk ZnO, respectively. The role of cobalt as in situ substrate-cum-dopant has been substantiated by analyzing the characterization and photocatalytic test results. This work is expected to open the door for low energy intensity single-step facile synthesis of a number of materials with metastable states for host of optoelectronic, energy, environment and spintronics applications.

Appendix A. Supplementary data

Supplementary data associated with this article can be found, in the online version, at http://dx.doi.org/10.1016/j.apcatb.2013.07.048.

References

[1] L. Pueyo, S. Siroky, S. Landsmann, M.E.V.D. Berg, M.R. Wagner, J.S. Reparaz, A. Hoffmann, S. Polarz, Chemistry of Materials 22 (2010) 4263–4270.

[2] A. Ashrafi, C. Jagadish, Journal of Applied Physics 10 (2007) 071101.

[3] Y. Jin, J. Wang, B. Sun, J.C. Blakesley, N.C. Greenham, Nano Letters 8 (2008) 1649–1653.

[4] P. Caroff, K.A. Dick, J. Johansson, M.E. Messing, K. Deppert, L. Samuelson, Nature Nanotechnology 4 (2009).

[5] K.W. Sun, J.X. Wang, Nano Letters 8 (2008) 1884–1889.

[6] F. Lu, W. Cai, Y. Zhang, Advanced Functional Materials 18 (2008) 1047–1056.

[7] L.J. Zhang, J. Qiangang, J. Li, J. Zhou, W.P. Cai, J. Cheng, W. Xu, G. Yin, X. Wu, Z. Jiang, S. Zhang, Z.Y. Wu, Chemical Communications 48 (2012) 91–93.

[8] Z.L. Wang, J. Song, Science 312 (2006).

[9] A.B.M.A. Ashrafi, A. Ueta, A. Avramescu, H. Kumano, Applied Physics Letters 76 (2000).

[10] A.B.M.A. Ashrafi, A. Ueta, H. Kumano, I. Suemune, Y.W. Ok, T.Y. Seong, Applied Physics Letters 79 (2001) 470.

[11] A. Ashrafi, Applied Surface Science 255 (2008) 2342–2346.

[12] G.H. Lee, T. Kawazoe, M. Ohtsu, Solid State Communications 124 (2002) 163–165.

[13] G.H. Lee, T. Kawazoe, M. Ohtsu, Applied Surface Science 239 (2005) 394–397.

[14] S.K. Kim, S.Y. Jeong, C.R. Cho, Applied Physics Letters 82 (2003) 4.

[15] L. Xu, Y. Su, Y. Chen, H. Xiao, L.A. Zhu, Q. Zhou, S. Li, Journal of Physical Chemistry B 110 (2006) 6637–6642.

[16] L.P. Snedeker, A.S. Risbud, O. Masala, J.P. Zhang, R. Seshadri, Solid State Sciences 7 (2005) 1500–1505.

[17] Y.Z. Yoo, Y. Osaka, T. Fukumura, Z. Jin, M. Kawaski, H. Koinuma, T. Chikyow, P. Ahmet, A. Setoguchi, S.F. Chichibu, Applied Physics Letters 78 (2001) 616.

[18] H. Kumano, A.A. Asharafi, A. Ueta, A. Avramescu, I. Suemune, Journal of Crystal Growth 214/215 (2000) 280.

[19] I. Suemune, A.B.M.A. Ashrafi, M. Ebihara, M. Kurimoto, H. Kumano, T.Y. Seong, B.J. Kim, Y.W. Ok, Physical Status Solidi B 241 (2004) 640.

[20] L. Lazzarini, G. Salviati, F. Fabbri, M. Zha, D. Calestani, A. Zappettini, T. Sekiguchi, B. Dierre, ACS Nano 3 (2009) 3158–3164.

[21] W.H. Chiu, C.H. Lee, H.M. Cheng, H.F. Lin, S.C. Liao, J.M. Wu, W.F. Hsieh, Energy & Environmental Science 2 (2009) 694–698.

[22] P.X. Gao, Y. Ding, W. Mai, W.L. Hughes, C. Lao, Z.L. Wang, Science 309 (2005).

[23] R.G. Nair, S. Paul, S.K. Samdarshi, Solar Energy Materials & Solar Cells 95 (2011) 1901–1907.

[24] R.G. Nair, A.M. Tripathi, S.K. Samdarshi, Energy 36 (2011) 3342–3347.

[25] R.G. Nair, J.K. Roy, S.K. Samdarshi, Solar Energy Material and Solar cell 105 (2012) 103–108.

[26] G.H. Lee, Y. Yamamoto, M. Kourogi, M. Ohtsu, Thin Solid Films 386 (2001) 117.

[27] C. Yeh, S. Wei, A. Zunger, Physical Review B 50 (1994) 2715.

[28] V. Eskizeybek, F. Sarı, H. Gülce, A. Gülce, A. Avcı, Applied Catalysis B: Environmental 119–120 (2012) 197–206.

[29] X. Qiu, G. Li, L. Li, X. Fu, Nanotechnology 19 (2008) 215703.

[30] M.G. Nair, M. Nirmala, K. Rekha, A. Anukaliani, Material Letters 65 (2011) 1797–1800.

[31] M.J. Redman, E.G. Steward, Nature 193 (1962) 867.

[32] R.W. Grimes, A.N. Fitch, Journal of Materials Chemistry 1 (1991) 461.

[33] Y. Yang, Y. Jin, H. He, Q. Wang, Y. Tu, H. Lu, Z. Ye, Journal of the American Chemical Society 132 (2010) 13381–13394.

[34] R. Elilarassi, G. Chandrasekaran, Journal of Materials Science: Materials in Electronics 24 (2013) 96–105.

[35] Y. Lu, Y. Lin, T. Xie, S. Shi, H. Fan, D. Wang, Nanoscale 4 (2012) 6393.

[36] S.H. Su, J.H. Lai, H.H. Chen, T.-H. Lee, Y.J. Hsu, R.L. Wang, J.C.A. Huang, Journal of Physical Chemistry C 116 (2012) 9917–9924.

[37] M.P. Hyman, E. Martono, John M. Vohs, Journal of Physical Chemistry C 114 (2010) 16892–16899.

[38] X. Wang, J. Xu, B. Zhang, H. Yu, J. Wang, X. Zhang, J. Yu, Q. Li, Advanced Materials 18 (2006) 2476–2480.

[39] X. Wang, R. Zheng, Z. Liu, H. Ho, J. Xu, S.P. Ringer, Nanotechnology 19 (2008) 455702.

[40] Y. Lu, Y. Lin, D. Wang, L. Wang, T. Xie, T. Jiang, Nano Research 4 (2011) 1144–1152.

[41] Q. Xiao, J. Zhang, C. Xiao, X. Tan, Material Science Engineering B 142 (2007) 121–125.

[42] J.M. Yuk, K. Kim, Z. Lee, M. Watanabe, A. Zettl, T.W. Kim, Y.S. No, W.K. Choi, J.Y. Lee, ACS Nano 4 (2010) 2999–3004.

[43] Y. Yan, G.M. Dalpian, M.M.A. Jassin, S.H. Wei, Physical Review B 70 (2004) 193206.